Simulating the spatially-dependent frequency response of arbitrary-shape acoustic detectors for optoacoustic imaging

Amir Rosenthal, Vasilis Ntziachristos, and Daniel Razansky
Institute for Biological and Medical Imaging, & Chair for Biological Imaging Technische Universität of München and Helmholtz Zentrum München, Ingolstädter Landstraβe 1, 85764 Neuherberg, Germany

ABSTRACT

One of the major challenges of optoacoustic imaging is that it involves relatively weak acoustic signals, which need to be detected with high signal-to-noise ratio (SNR). Because the SNR is generally proportional to the area of the detector's face, large detectors are commonly used. Although the use of such detectors improves the SNR, it may lead to significant signal distortion resulting in artifacts in the reconstructed optoacoustic image. In this work we developed a method for simulating the spatially dependent frequency response of acoustic detectors with arbitrary surface shapes. The frequency response is incorporated into a forward model for optoacoustic propagation. Our method can be used for designing detectors with desired properties and reducing reconstruction artifacts caused by the response of finite-size detectors.

Keywords: optoacoustics, photoacoustics, acoustic sensors, acoustic modeling.

1. INTRODUCTION

Optoacoustic imaging is a non-invasive hybrid imaging method for high-resolution mapping of optical absorption in tissues[1-9]. The ability of optoacoustics to image tissue has been shown by visualizing vascular anatomy[2], tumor angiogenesis[10], as well as functional imaging of blood oxygenation[11] in living tissues of small animals and humans. It has been also shown that common fluorochromes, such as fluorescent proteins or fluorescent molecular probes can be resolved with high specificity when employing illumination at several optical wavelengths using multispectral optoacoustic tomography (MSOT)[3,12].

Optoacoustic imaging is performed by illuminating an optically absorbing object with short high-power laser pulses and measuring the subsequent ultrasound fields emanating from within the object. Various detector geometries are used in the detection, which can be largely divided into three categories: cylindrically focused detectors[1-3], spherically focused detectors[4-6], and flat detectors[7-9]. The geometry of the detector is chosen according to the given imaging scenario to optimize image fidelity. The choice of detector geometry affects the dependence of the magnitude and bandwidth of its acoustic response on the location of the optoacoustic source.

The measured acoustic fields are used to form an image of the optical absorption within the imaged object by means of inversion algorithms[13,14]. Despite the profound effect the detector geometry may have on the detected acoustic field, it is often assumed in the inversion that the detector can be approximated by a point detector in which the sensitivity is not spatially dependant. In the case of back-projection algorithms, generalization to focused detectors was obtained using the virtual-detector approach[4]. However, this approach is limited in resolution by the focal width of the detector. In addition, no generalization to flat detector has been proposed.

Photons Plus Ultrasound: Imaging and Sensing 2011, edited by Alexander A. Oraevsky, Lihong V. Wang,
Proc. of SPIE Vol. 7899, 78992S · © 2011 SPIE · CCC code: 1605-7422/11/$18 · doi: 10.1117/12.874082

In order to accurately account for the geometry of the detector in the inversion, model-based algorithms should be used. In these algorithms, the forward acoustic problem is modeled, allowing the calculation of the acoustic fields for any given optoacoustic source. The forward model is then used in an optimization algorithm to find the optoacoustic image whose corresponding acoustic signals match those which were measured. The geometry of the detector can be integrated in the forward model by convolving the image with the shape of the detector[9]. However, this method was only demonstrated for flat detectors in a translational scanning geometry, in which the shape of the detector fits the grid on which the optoacoustic image is represented. In other geometries, numerical convolution might result in artifacts in the calculated acoustic signal. Additionally, spatial convolution increases the size of the image, which in the case of large detectors may significantly reduce numerical efficiency.

Recently, a numerically efficient model-based inversion algorithm, termed interpolated-matrix-model-inversion (IMMI) was developed[14]. The method is based on building a forward-model matrix connecting the optoacoustic image and the measured acoustic signals. One of the advantages of this approach is the ability to include linear effects in the model. In Ref. [14], a spatially constant frequency response was included in the model, whereas in Ref. [15], the spatially-dependent effect of non-uniform illumination was modeled. In both cases, the inclusion of additional effects led to an improved image reconstruction.

In this paper we present an efficient and accurate method for integrating the effect of the sensor geometry in IMMI. In contrast to the method presented in Ref. [9], no spatial convolution is performed. Instead, the temporal response of the detector is calculated for point sources on every pixel on the grid. The calculated responses are then integrated in the model by performing convolution in the time domain. The advantage of this approach is that it circumvents numerical difficulties involved with spatial convolution in non-rectangular detection geometries, e.g. focused detector.

The spatially dependent impulse response can be calculated for acoustic detectors of any shape using an analytical solution to the field equation obtained for a line acoustic detector. The detector is then approximated by a set of line detectors. The response of the detector is integrated in the optoacoustic model, thus allowing one to calculate the response of arbitrary-shape detector to any optoacoustic source. The method is demonstrated in numerical simulations for flat and focused detectors in 2D.

The ability to simulate the effect of the detector geometry on the detected acoustic signal can be utilized for the design of acoustic detectors for optoacoustic imaging. Specifically, the shape of the detector can be optimized to obtain maximum response for images with features similar to those imaged. In addition, the inclusion of spatially-dependent frequency response of the detector can improve the quality of the optoacoustic reconstruction using IMMI, similarly to previously published generalizations.

The paper is organized as follows: In section II we present the theoretical background for optoacoustic imaging; in section III we develop the theory for calculating the frequency response of acoustic detectors and for integrating it in the optoacoustic model; in section IV we present numerical simulations of our methods; in section V we compare experimental results to theoretical predictions; and in section IV we discuss the results.

2. THEORETICAL BACKGROUND

In an acoustically homogenous medium, under the condition of thermal confinement[1], the optoacoustically induced pressure wave *p(r,t)* obeys the following equation[16]:

$$\frac{\partial^2 p(r,t)}{\partial t^2} - v^2 \nabla^2 p(r,t) = \Gamma H_r(r) \frac{\partial H_t(t)}{\partial t}, \tag{1}$$

where v and ρ are velocity of sound in tissue and its density, Γ is the Grüneisen parameter, and $H(r,t) = H_r(r)H_t(t)$ is the amount of energy absorbed in the tissue per unit volume and per unit time, which is the source for the acoustic fields.

We start our treatment by using the solution to Eq. 1 for a delta-function source, i.e. we substitute the right-hand side of the equation with $\delta(r)\delta(t)$. The solution to Eq. 1 in that case is a spherical delta function[17]:

$$p_\delta(r,t) = \frac{\delta(|r| - vt)}{4\pi|r|} \tag{2}$$

Since Eq. 1 is linear, its solution can be represented as a superposition of the fundamental solution given in Eq. 2:

$$p(r,t) = \frac{\Gamma}{4\pi} \int \frac{\delta\big(|r-r'| - v(t-t')\big)}{|r-r'|} H_r(r') \frac{\partial}{\partial t} H_t(t') dr' dt'. \tag{3}$$

Assuming that the laser pulse is significantly shorter than the temporal resolution of the detection, the function $\mathrm{H_t(t)}$ can be substituted by a temporal delta function, yielding:

$$p(r,t) = \frac{\Gamma}{4\pi} \int \frac{\delta'(|r-r'| - vt)}{|r-r'|} H_r(r') dr', \tag{4}$$

where δ' is the derivative of Dirac's delta function. Further simplification leads to the following equation:

$$p(r,t) = \frac{\Gamma}{4\pi v} \frac{\partial}{\partial t} \int_{|r-r'|=vt} \frac{H_r(r')}{|r-r'|} dr', \tag{5}$$

in which the integration is performed on the sphere defined by $|\mathrm{r} - \mathrm{r}'| = \mathrm{vt}$. If the optoacoustic sources are assumed to be located on a plane, the integration is performed on arc.

Equation 5 is commonly used to calculate the acoustic fields generated by an arbitrary optoacoustic source. The discretization of Eq. 5 is given in Ref. [14] and lead to the following matrix relation:

$$p = \mathbf{M}z \tag{6}$$

Where p is a column vector representing the acoustic fields measured at a position r, for a set of times $\{t_i\}$ (i=1…I): $p_i = p(r, t_i)$; z is a column vector representing the values of the optoacoustic source on the grid $z_j = H(r_j)$ (j=1:…J); and M is the model matrix for a point detector positioned at r.

In the case of a finite size detector, the response of the detector is obtained by integrating $\mathrm{p(r,t)}$ over the surface of the detector:

$$p_{detect}(t) = \int p(r,t) D(r) dr, \tag{7}$$

where

$$D(r) = \begin{cases} 1 & r \in \text{detector area} \\ 0 & \text{else} \end{cases}. \tag{8}$$

In order to numerically calculate Eq. 7, the integral in Eq. 5 should be evaluated for different points over the detector's surface. This procedure would require calculating the model matrix M for each point on the detector's surface, leading to high computational complexity. In order to reduce the complexity, a different expression for $p_{det}(t)$ was proposed in Ref. [9] :

$$p_{det}(t) = \frac{\Gamma}{4\pi v}\frac{\partial}{\partial t}\int_{|r-r'|=vt}\frac{D*H_r(r)}{|r-r'|}dr', \tag{9}$$

where * denotes the convolution operator. The advantage of using the expression in Eq. 9 is that it requires calculating the model matrix only once.

While the convolution operation in Eq. 9 can be performed with high numerical efficiency, it is prone to numerical errors if the shape of the detector is not accurately represented on the square grid on which $H_r(r)$ is given, e.g. curved detectors. In such cases, in order to minimize the errors, the grid resolution should be increased beyond the imaging resolution of the system, significantly increasing the computational complexity.

3. THE RESPONSE OF ARBITRARY-SHAPE DETECTORS

In this section we present a semi-analytical solution to simulate the response of arbitrary-shape acoustic detectors. The solution is based on finding an analytical expression to the response of a flat 2D detector to a point source. The response is given in the time-domain and can be integrated into the model matrix M by using temporal convolution. The response of an arbitrary-shape detector can be simulated by approximating the detector by a series of flat detectors.

The source-detector geometry of a flat detector and a delta source is shown in Fig. 1, where a is the width of the detector, $r = (x, y)$ is the location of the detector's center, $r' = (x', y')$ is the location of the source, and θ is the tilt angle of the detector. The detector's response is obtained by integrating Eq. 2 over the detector's length. For $\theta = 0$, the detected pressure field is given by

$$p_f(t, r', r, \theta = 0) = \int_{y-y'-a/2}^{y-y'+a/2}\frac{\delta\left(\sqrt{(x-x')^2+\hat{y}^2}-vt\right)}{4\pi v\sqrt{(x-x')^2+\hat{y}^2}}d\hat{y}. \tag{10}$$

In order to calculate the integral in Eq. 10, we first calculate the temporal anti-derivative of $p(t)$:

$$P_f\left(t, r', r_f, \theta = 0\right) = \frac{1}{v}\int_{y_f-y'-a/2}^{y_f-y'+a/2}\frac{H\left(\sqrt{(x-x')^2+\hat{y}^2}-vt\right)}{4\pi v\sqrt{(x_f-x')^2+\hat{y}^2}}d\hat{y}. \tag{11}$$

where H is the Heaviside step function. A closed-form expression to P_f and p_f are given in Appendix I.

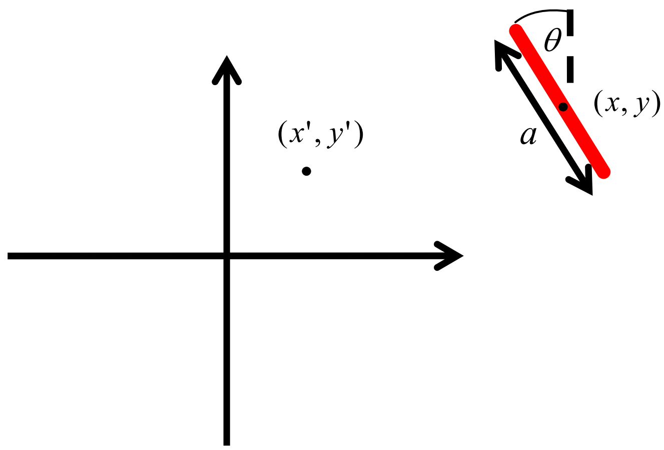

Figure 1. A schematic description of a point source and a flat detector in 2D.

In the case of an arbitrary shape detector, the detector's surface is approximated by a series of flat detectors defined by their specific location and orientation$\{(\mathrm{r}_n, \theta_n)\}_{n=1}^{N}$. The response of the detector is then readily obtained by summing the responses of the flat detectors

$$p_{arb}(t, r') = \sum_{n=1}^{N} p_f(t, r', r_n, \theta_n) \tag{12}$$

In analogy to Eq. 5, the acoustic field detected by an arbitrary-shape detector from an arbitrary optoacoustic source is given by

$$p(t) = \frac{\Gamma}{4\pi\nu}\frac{\partial}{\partial t}\int p_{arb}(t, r')H_r(r')dr'. \tag{13}$$

We note that the integration is performed over all values of r' and not only on a single arc. In contrast to Eq. 9, in Eq. 13 the source $H_r(r')$ is not spatially convolved but rather multiplied by a function which is known analytically.

In order to discretize Eq. 13, we first bring it to the form of Eq. 5:

$$p(t) = \frac{\Gamma}{4\pi}\int |r - r'| p_{arb}\left(t + \frac{|r-r'|}{\nu}, r'\right) * \frac{\delta'(|r-r'|-\nu t)}{|r-r'|} H_r(r')dr'. \tag{14}$$

where the convolution is performed in the time domain. Thus, to obtain the signal measured by a finite-size detector, for each value of r', the contribution of the optoacoustic source to the signal measured by a point detector should be convolved with the function$|\mathrm{r} - \mathrm{r}'|\mathrm{p}_{\mathrm{arb}}(\mathrm{t} + |\mathrm{r} - \mathrm{r}'|/\nu, \mathrm{r}')$. In the discretized equations, the contribution of the optoacoustic source at a point r_j to the acoustic signal measured by a point detector is given by the *j*th row of the matrix **M**. Thus, to obtain the model matrix for a finite-size detector, for all values of *j*, the *j*th row of the matrix M should be convolved with $|\mathrm{r} - \mathrm{r}_j|\mathrm{p}_{\mathrm{arb}}(\mathrm{t} + |\mathrm{r} - \mathrm{r}_j|/\nu, \mathrm{r}_j)$.

4. NUMERICAL SIMULATIONS

In this section we demonstrate our method for calculating the response of two commonly used detector geometries: flat detector and focused detector. The responses of both detectors were integrated into the model matrix of a point detector calculated using the method in Ref. [14]. All the simulations were performed in 2D with geometrical parameters similar to what has been used in previous studies. The simulation was performed over a 100x100 grid with a resolution of 200μm with a detector positioned 4 cm from the center of the imaged area. The focused detector had a focal length of 4 cm and was approximated by 30 flat detectors. The two geometries are shown in Fig. 2.

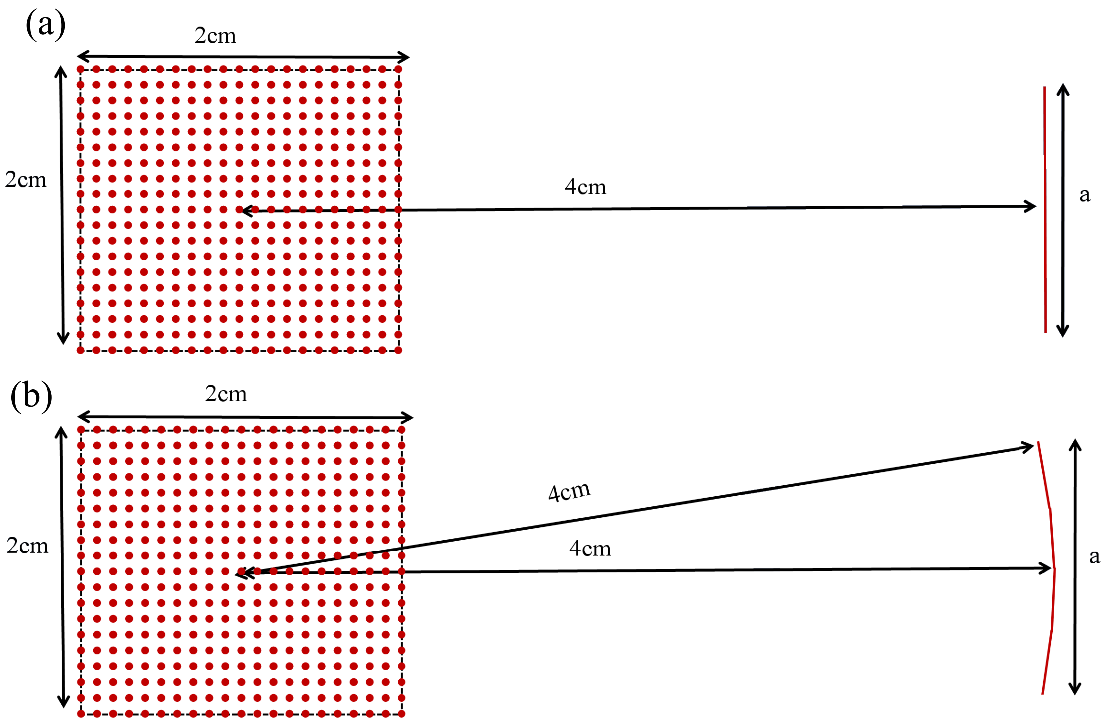

Figure 2. A schematic description of the geometry used in the numerical simulations for (a) flat and (b) focused

In the first example, we calculated the spatially dependent frequency responses of flat and focused detectors. The frequency response was calculated by taking the Fourier transform of p_{arb} for every coordinate on the grid. The simulations were performed for 2 values of the sensor length a 0.65 cm and 1.3cm. The bandwidth of the responses was defined according to the following formula:

$$BW = \sqrt{\frac{\int_{-\infty}^{\infty} \left|P(f) f\right|^2 df}{\int_{-\infty}^{\infty} \left|P(f)\right|^2 df}} . \tag{15}$$

Figures 3a and 3b show the bandwidth map of the flat detector for a=0.65cm and a=1.3cm, respectively. For both values, the high bandwidth region has approximately the same width as the detector. The wider detector exhibited a lower bandwidth as expected due to spatial averaging. Figures 3c and 3d show the bandwidth map of the focused detector for a=0.65cm and a=1.3cm, respectively. As expected, the region around the focal line of the detector has a higher bandwidth than the areas outside it. The larger detector exhibited a tighter focus and less variation in bandwidth along the focal line. The maximum value of the bandwidth was limited by the temporal resolution used for the calculations.

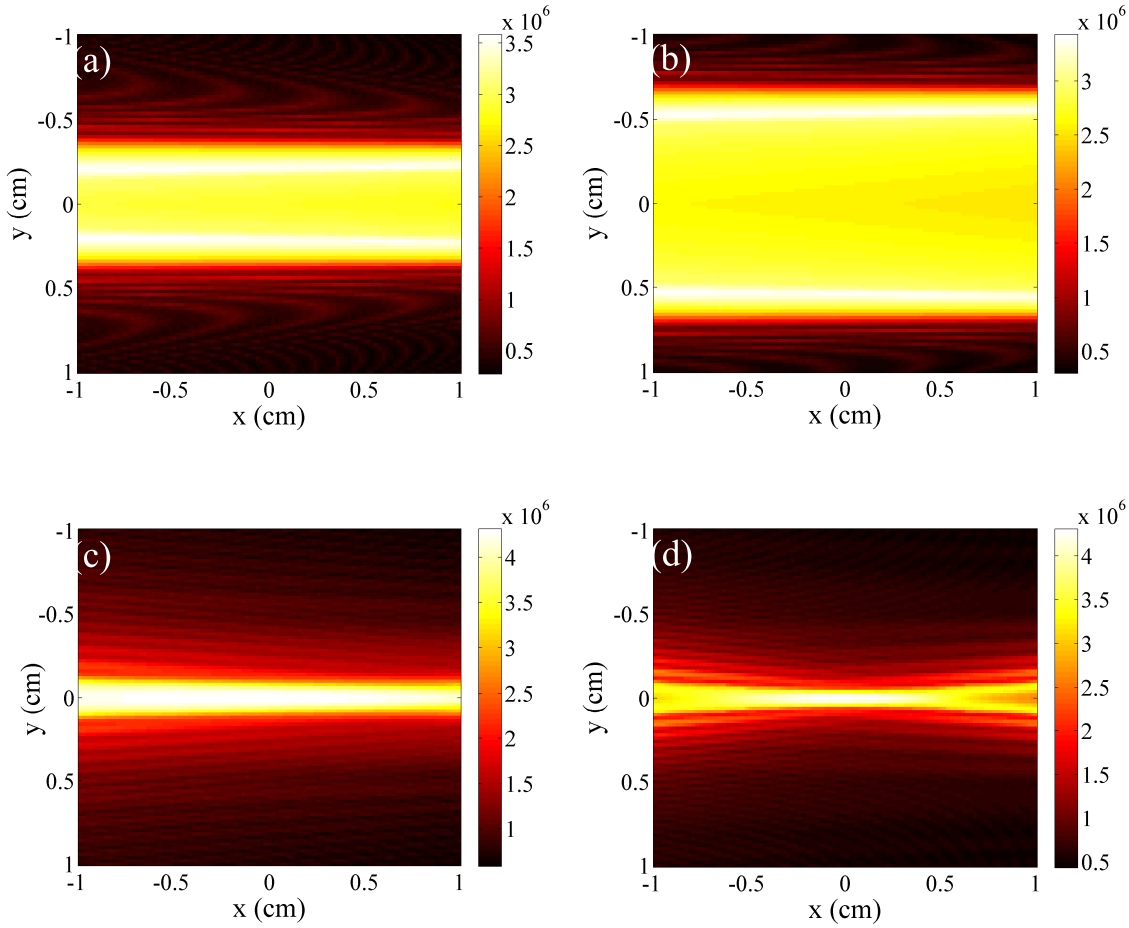

Figure 3. A map of the effective bandwidth, as defined in Eq. 15, of the detection calculated for the geometry of Fig. 2a with (a) a=0.65cm and (b) a=1.3cm and for the geometry of Fig. 2b with (c) a=0.65cm and (d) a=1.3cm. The frequency response was calculated for each point on the grid using Eq. (12) and (A7).

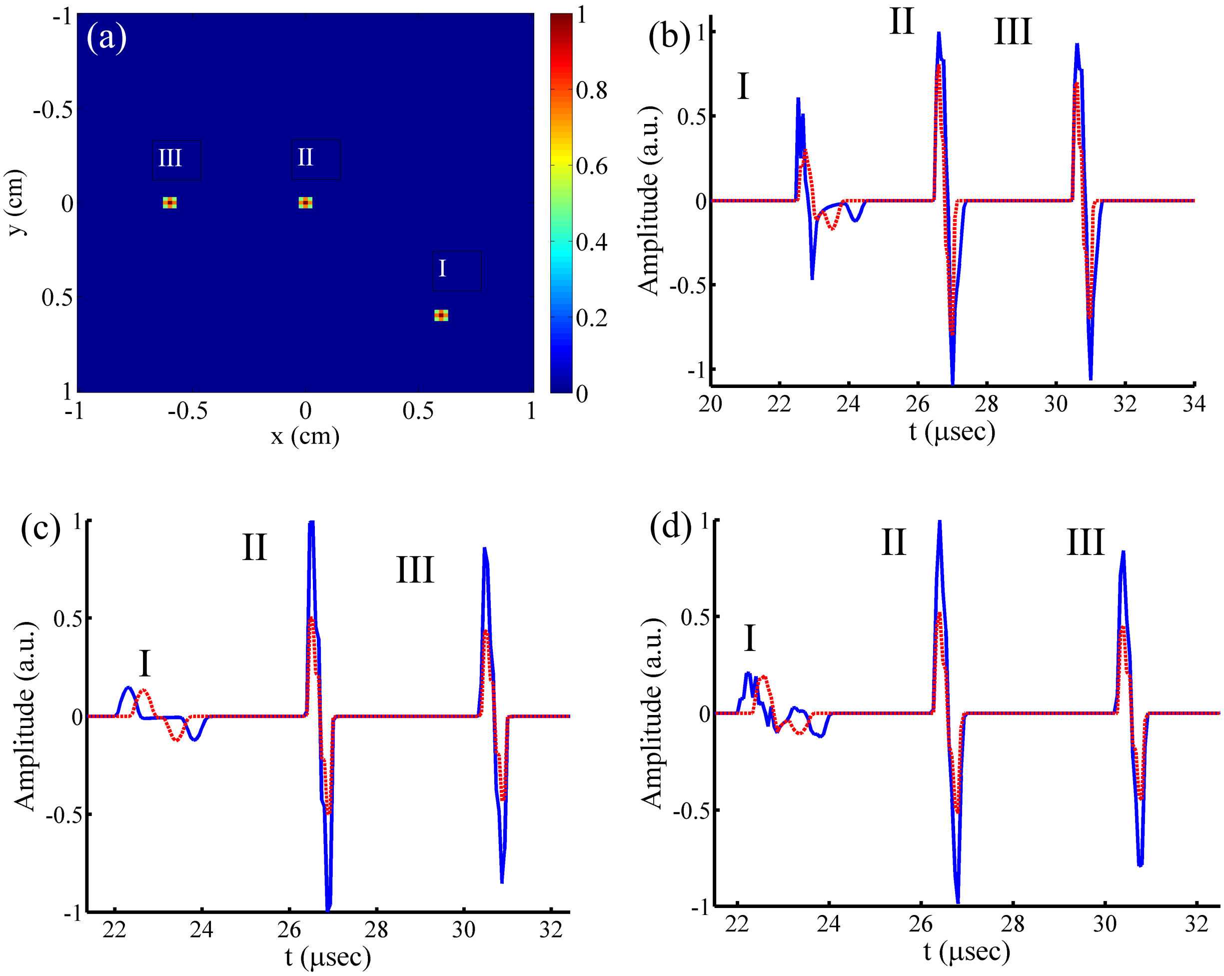

Figure 4. (a) An optoacoustic test image composed of 3 point source for which acoustic fields were calculated. The response was calculated using the temporal-convolution method for a (b) flat and (c) focused transducer. In addition, the response for the focused transducer was calculated using (d) the spatial-convolution method described in Ref [9]. The response was calculated for two detector sizes: a=1.3cm (solid-blue curve) and a=0.65cm (dashed-red curve). The figure shows numerical artifacts in the response calculated using the spatial-convolution method for source I.

In the next example, we calculated the response of the flat and focused detectors to the image shown in Fig. 4a. Figure 4b and 4c respectively show the responses for the flat and focused calculated with a=1.3cm (solid-blue curve) and a=0.65cm (dashed-red curve). The benefits of large focused detectors are clearly visible in the figure. Although the larger focused detector has a slightly lower bandwidth at the edges of the focal line, as compared to the smaller detector, it still achieves approximately twice the signal for detector for sources I and II without signal distortion. In addition, the rejection of source III outside the focal line is not reduced in the larger detector. In contrast, in the case of the flat detector, the larger detector only gave a marginally stronger signal than that of the smaller detector for sources I and II.

This increase came at a price of increased signal duration, which is clearly visible in the figure. Additionally, a much stronger distortion to the bipolar signal of source III is obtained for the larger detector.

Figure 4d shows the responses to the image shown in Fig. 4a for the focused detectors, obtained using the spatial-convolution method described in Ref. [9]. Because the spatial convolution increased the support of the image, the grid over which the simulation was performed was increased to 150x150, whereas the resolution was maintained at 200µm. The figure shows that for the in-focus targets, the results are similar to the temporal-convolution method discussed in this work. However, the signal from the out-of-focus target suffered from significant distortion. First, in contrast to expected result obtained by the time-convolution method – where all the contributions of different parts of the focused transducer but the edges cancelled each other out – no signal cancellation was obtained. Additionally, the signal obtained for a=1.3 mm contains discontinuities owing to numerical errors. These discontinuities can be eliminated by increasing the image resolution to 100µm, but at the cost of higher numerical complexity. We note that increasing the resolution only contributed to the smoothness of the signals and did not lead to the result obtained by the time-domain convolution method.

5. DISCUSSION

In this paper we developed a new method for integrating the effect of the detector geometry in optoacoustic forward simulations. Although this effect can significantly alter the detected acoustic fields it is usually ignored in inversion algorithms, which may lead to reconstruction errors. While back-projection algorithms are not inherently equipped to incorporate the effect of detector geometry, model-based algorithms can theoretically include the effect of any detector geometry.

Our method is based on calculating the spatially dependent impulse response of the detector which results from its geometry. An analytical solution was developed for a line detector. The shape of an arbitrary 2D detector can then approximated by approximating the detector by a set of line detectors. The impulse response is then integrated in the model matrix by convolving the acoustic signal obtained for each pixel in the image with its corresponding impulse response.

Our temporal-convolution method was compared in numerical simulations to the spatial-convolution method described in Ref [9]. In Ref. [9] the geometry of the detector was integrated in the forward optoacoustic problem by convolving the optoacoustic image with the shape of the detector. Although the mathematical formulation of the spatial-convolution method is exact, its direct numerical implementation involves difficulties which may result in high complexity and errors. One difficulty demonstrated in this work is simulating the response of focused detectors to out-of-focus small targets. For these targets the field summation over the surface of the detector should cancel all the contributions but those originating from the detector edges. However, because the detector is discretizied, the summed bi-polar optoacoustic signals do not get perfectly cancelled out. In contrast, our temporal-convolution method accurately simulated the acoustic response in that case.

The method developed in this work can be utilized for the design of acoustic detectors for optoacoustic imaging. Specifically, the shape of the detector can be optimized to obtain maximum response for images with features similar to those imaged. In addition, the inclusion of spatially-dependent frequency response of the detector can improve the quality of the optoacoustic reconstruction using IMMI, similarly to previously published generalizations.

REFERENCES

[1] Kruger R. A., Liu P., Fang Y. R., Appledorn C. R., “Photoacoustic ultrasound (PAUS)--reconstruction tomography,” Med Phys. 22, 1605-1609 (1995).

[2] Wang X., Pang Y., Ku G., Xie X., Stoica G., and Wang L. H. V., “Noninvasive laser-induced photoacoustic tomography for structural and functional in vivo imaging of the brain,” Nat. Biotechnol. 21, 803-806 (2003).

[3] Ma R., Taruttis A., Ntziachristos V., and Razansky D., “Multispectral optoacoustic tomography (MSOT) scanner for whole-body small animal imaging,” Opt. Express, 17, 21414-21426 (2009).

[4] Li M.L., Zahng H.E., Maslov K., Stoica G., Wang L.V., “Improved in vivo photoacoustic microscopy based on a virtual-detector concept,” Opt. Lett. 31, 474-476 (2006).

[5] Zhang H.F, Maslov K., Stoica G., and Wang L.V., “Functional photoacoustic microscopy for high-resolution and noninvasive in vivo imaging,” Nature Biotechnology, 24, 848-851 (2006).

[6] Bost W., and Lemor R. M., “Photoacoustic Microscopy for High-resolution Imaging,“ J. Acoust. Soc. Am. 123, 3370-3375 (2008).

[7] Kruger R.A., Kiser Jr W. L. , Reinecke D.R., and Kruger , “Thermoacoustic computed tomography using a conventional linear transducer array,” Med. Phys., 30, 856-60 (2003).

[8] Manohar S., Kharine A., van Hespen J. C. G., Steenbergen W., and van Leeuwen T. G., “The Twente Photoacoustic Mammoscope: system overview and performance“ Phys. Med. Biol. 50, 2543-2557 (2005).

[9] Köstli K. P. and Beard P.C., “Two-dimensional photoacoustic imaging by use of Fourier-transform image reconstruction and a detector with an anisotropic response,” App. Opt. 42, 1899-1901 (2003).

[10] Siphanto R. I., Thumma K. K., Kolkman R. G. M., van Leeuwen T. G., de Mul F. F. M., van Neck J. W., van Adrichem L. N. A., and Steenbergen W., “Serial noninvasive photoacoustic imaging of neovascularization in tumor angiogenesis,” Opt. Express 13, 89–95 (2005).

[11] Laufer J., Delpy D., Elwell C., and Beard P., “Quantitative spatially resolved measurement of tissue chromophore concentrations using photoacoustic spectroscopy: application to the measurement of blood oxygenation and haemoglobin concentration,” Phys. Med. Biol., 52, 141–168 (2007).

[12] Razansky D., Distel M., Vinegoni C., Ma R., Perrimon N., Köster R. W. and Ntziachristos V., “Multi-spectral optoacoustic tomography of deep-seated fluorescent proteins in vivo,” Nature Photonics, 3, 412 – 417 (2009).

[13] Xu M. and Wang L. V., "Universal back-projection algorithm for photoacoustic-computed tomography," Phys. Rev. E 71(1), 016706 (2005).

[14] Rosenthal A., Razansky D., and Ntziachristos V., “Fast semi-analytical model-based acoustic inversion for quantitative optoacoustic tomography”, IEEE Trans. Med. Imaging, 29, 1275 - 1285 (2010).

[15] Jetzfellner T., Rosenthal A., Buehler A., Dima A., Englmeier K. H., Ntziachristos V., and Razansky D., "Optoacoustic tomography with varying illumination and non-uniform detection patterns," J. Opt. Soc. Am. A, 27, 2488-2495 (2010).

[16] Cox B. T., Kara S., Arridge S. R., and. Beard P. C, “k-space propagation models for acoustically heterogeneous media: application to biomedical photoacoustics,” The Journal of the Acoustical Society of America 121, 3453-3464 (2007).

[17] Blackstock D. T., [Fundamentals of physical acoustics], D.T., John Wiley & Sons, New York, NY (2000).